Anomalous Quantum Dynamics in Lossy Nonlocal System

Liwei Qiao[1], Wei Zhang[1,2,3*], and Kaiye Shi[1,2,4,5*]

[1]*School of Physics and Key Laboratory of Quantum State Construction and Manipulation (Ministry of Education), Renmin University of China, Beijing 100872, China*
[2]*Beijing Academy of Quantum Information Sciences, Beijing 100193, China*
[3]*Beijing Key Laboratory of Opto-electronic Functional Materials and Micro-nano Devices, Renmin University of China, Beijing 100872, China*
[4]*State Key Laboratory for Mesoscopic Physics, School of Physics, Frontiers Science Center for Nano-optoelectronics, & Collaborative Innovation Center of Quantum Matter, Peking University, Beijing 100871, China*
[5]*Hefei National Laboratory, Hefei 230088, China*

(Received 1 September 2024; accepted manuscript online 5 November 2024)

The non-Hermitian skin effect and edge burst reflect the vital role of spatial boundaries in non-Hermitian systems from both static and dynamic perspectives. In this study, we investigate a non-Hermitian dissipative lattice with nonlocal coupling and demonstrate many interesting static and dynamic phenomena. In the case of global coupling with all sites coupled with each other, we observe anomalous hopping resonance, where a quantum walker initially placed at a single site almost completely escapes from the boundary of the system regardless of its initial position. In the case of non-global coupling, which is infinite-range coupling, the interplay between nonlocal hopping and the non-Hermitian skin effect results in the emergence of local bulk modes exhibiting a multipartite density distribution. The presence of local bulk modes induces the nontrivial dynamics of a quantum walker, which features multiple peaks of lost probability in spatially separated domains. Our findings demonstrate unique properties induced by nonlocal coupling in non-Hermitian systems.

DOI: 10.1088/0256-307X/41/12/120301

Introduction. Although quantum mechanics is essentially based on the assumption of hermiticity, non-Hermitian phenomena[1–7] are ubiquitous due to the inevitable exchange of energy and particle numbers between a real system and its environment. Compared to Hermitian systems, non-Hermitian systems are extremely sensitive to spatial boundary conditions. Specifically, when the periodic boundary condition is changed to an open-boundary condition, the original extended Bloch eigenstates accumulate at the system boundaries, leading to a phenomenon known as the non-Hermitian skin effect (NHSE).[8–12] The NHSE is a unique topological phenomenon in non-Hermitian systems, which is related to the winding of complex energy spectra.[13–16] Unlike the topology of wave functions in Hermitian systems,[17,18] which requires the existence of two or more energy bands, the NHSE occurs in a single-band system because it is a point-gap topology rather than a line-gap topology.[19]

Recently, the dynamics in dissipative lattices has attracted widespread theoretical[5,20] and experimental[21,22] attention. In particular, when there is a NHSE in a dissipative lattice,[23–27] a quantum walker moving in a lattice has a finite probability of escaping from the boundary even when its initial position is far from the boundary. This phenomenon, referred to as a non-Hermitian edge burst (NHEB), was first discovered in a non-Hermitian lattice with uniform dissipation[23,24] and subsequently in a non-Hermitian lattice with non-uniform dissipation.[25] Initially, the NHEB was attributed to the topological edge states. Subsequently, Xue *et al.* highlighted that edge bursts were caused by the interplay between NHSE and imaginary gap closing.[23] Recently, two experimental NHEB studies have been reported.[26,27]

Another frontier of lattice system research is the effect of long-range coupling. For several decades, attention has been primarily focused on systems with local or short-range couplings, such as local ϕ^4 field theories and nearest-neighbor couplings. In the past decade, models with long-range coupling have become increasingly relevant when describing experiments involving trapped ion setups,[28,29] polar molecules,[30,31] Rydberg atoms,[32] cold atoms in cavities,[33–35] superconductor qubit systems,[36] and artificial metamaterials.[37,38] The form of long-range coupling is generally regarded to be power-law decay, which induces novel nonlocal phenomena beyond short-range systems.[39–41] The bulk characteristics of such systems can generally be approximated by the Bloch Hamiltonian in general. Recently, a new form of long-range coupling has been proposed,[42] whose coupling strengths are uniform, and the coupling range is comparable to the system size. This long-range coupling is an infinite-range nonlocal coupling, i.e., the coupling range R goes to infinity with the system size N (the number of unit cells) in the thermodynamic limit. This type of nonlocal coupling causes the Bloch Hamiltonian to be unable to approximate the bulk characteristics of open-boundary systems, resulting in

*Corresponding author. Email: wzhangl@ruc.edu.cn; kaiye-sky@ruc.edu.cn
© 2024 Chinese Physical Society and IOP Publishing Ltd

novel phenomena that are extremely different from those of Bloch systems.

In this Letter, we investigate the dynamics of a quantum walker in a lossy lattice with nonlocal (infinite-range) hopping.[42] Nonlocal coupling can induce two interesting phenomena. On the one hand, if the ratio between the coupling range and the system size $(R+1)/N$ is greater than $1/2$, the system can have a complete edge burst in a specific region where the quantum walker almost completely decays at the boundary rather than its initial position. On the other hand, nonlocal coupling can induce a novel type of local bulk mode (LBM) featuring a multipartite spatial distribution, which induces multipeak behavior in both the density distribution and the loss probability of the quantum walker. These characteristic phenomena are generated by the combined effect of NHSE and nonlocal coupling.

Model. Our work begins with a non-Hermitian model with arbitrary-range hopping, as shown in Fig. 1(a). The real-space Hamiltonian requires

$$\begin{aligned} H = &\sum_j \Big[t_0(a_j^\dagger b_j + \text{H.c.}) - i\gamma b_j^\dagger b_j\Big] \\ &+ \sum_{l=1}^{R}\sum_j \Big[\frac{it_l}{2}(a_{j+l}^\dagger a_j - b_{j+l}^\dagger b_j) \\ &+ \frac{t_l}{2}(a_{j+l}^\dagger b_j + a_j^\dagger b_{j+l}) + \text{H.c.}\Big], \end{aligned} \tag{1}$$

where $a_j^\dagger$ ($b_j^\dagger$) denote the creation operators on the A (B) sublattices of the j-th unit cell and satisfy $a_j^\dagger|0\rangle = |j, A\rangle$ ($b_j^\dagger|0\rangle = |j, B\rangle$), t_0 denotes the intracell hopping, t_l denotes the hopping between the j-th and $(j+l)$-th cells, R represents the maximum hopping distance, and γ denotes the loss rate of the B sublattice. The Bloch Hamiltonian can be expressed as follows:

$$\mathcal{H}(k) = \sum_{l=1}^{R} t_l \cos(lk)\sigma_x + \left[\sum_{l=0}^{R} t_l \sin(lk) + \frac{i\gamma}{2}\right]\sigma_z - \frac{i\gamma}{2}I, \tag{2}$$

where σ's and I denote the Pauli matrices and the identity acting on the sublattices, respectively.

In the case of $R = 1$, the Hamiltonian Eq. (1) is a typical one-dimensional non-Hermitian lattice model without interactions, whose single-particle characteristics have been extensively discussed.[43] This Hamiltonian can be transformed into a lossy Su-Schrieffer-Heeger (SSH) model with asymmetric hopping[9] through a local unitary transformation $U = \bigoplus_j e^{-i\pi\sigma_{x,j}/4}$, which naturally supports NHSE (background loss does not affect the eigenstates). When $|t_0| < |t_1|$, the imaginary gap is closed, and the interplay with NHSE results in NHEB,[23] i.e., the quantum walker far from the boundary has a high probability of escaping at the boundary.

Another special case is $\gamma = 0$, where Eq. (1) reduces to a Hermitian SSH model with arbitrary-range hopping under the same unitary transformation $U = \bigoplus_j e^{-i\pi\sigma_{x,j}/4}$. The bulk characteristics of this system under open-boundary conditions cannot be approximated by its Bloch form if the hopping range R is comparable to N. This non-Bloch topological insulator exhibits in-gap edge modes and LBMs restricted to specific regions.[42] LBMs with multipartite mode distributions are a special class of eigenstates of Hermitian non-Bloch systems, which originate from the interplay between nonlocal coupling and the boundary effect. This novel bulk mode does not expand throughout the entire space similarly to Bloch states, nor is it localized at the boundaries of the system similarly to edge states. Instead, it exhibits an extensible distribution within multiple regions of the system and is characterized by the parameter $\alpha \equiv (R+1)/N$. Specifically, LBMs are distributed in the spatial dimension in the regions of $j \in [1,\ N-(m-1)\alpha N]$, $[1+R,\ N-(m-2)\alpha N]$,..., $[1+(m-1)R,\ N]$ with $m = [1/\alpha]$. Here, $[1/\alpha]$ represents the integer rounding up from $1/\alpha$ and the distance between two adjacent regions is R. Both the multipartite localized distribution and the step-like dependence on the coupling range indicate that the LBMs may be rooted in the interference of the reflected wave from the boundary.[42] Hereafter, these spatial domains with nonzero LBM density profiles are referred to as LBM regions, and the other domains are referred to as non-LBM regions.

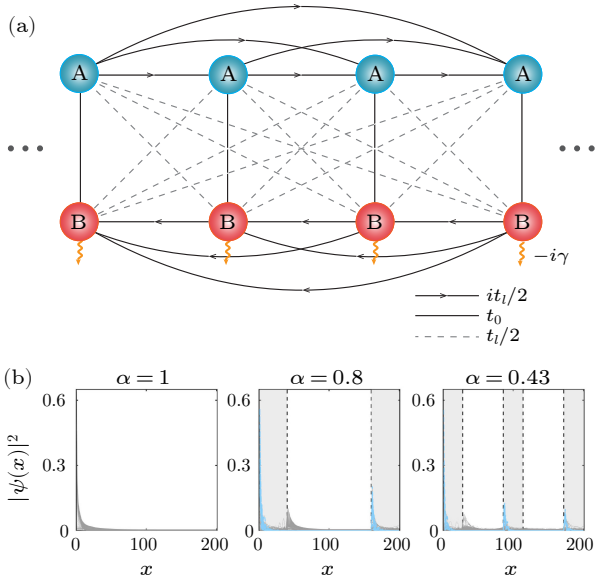

Fig. 1. (a) Model illustration. Each unit cell contains two subunits labeled A and B. The solid lines indicate the intracell hoppings t_0, and the arrowed and dotted lines indicate the intercell hoppings between sites in the j-th unit cell and those in the $(j+l)$-th unit cell, where $0 \le l \le R$ and R represents the maximal range of hopping. Dissipation with rate γ occurs from each site on the B sublattice. (b) All eigenstate density distributions (modulus square) of the Hamiltonian in real space with $\alpha = 1$ (left), 0.8 (middle), and 0.43 (right). The non-Hermitian LBMs in the shaded LBM regions are indicated by blue lines. The gray lines represent bulk modes other than non-Hermitian LBMs, which are generally distributed throughout the entire system. The other parameters used here are $N = 200$, $\gamma = 0.2$, $t_0 = 0.3$, $t_l = 0.5$ for $1 \le l \le \alpha N - 1$.

For the general case of $\gamma \neq 0$ and a finite $\alpha < 1$, the interplay between NHSE and nonlocal coupling may lead to more diverse and interesting physical phenomena. For simplicity, we assume that t_0 and t_l are both real positive

numbers and set $t_l = t_1$ for all $0 < l \leq R$ in the following discussion. The real-space density profiles of all eigenstates at different α are shown in Fig. 1(b), revealing the effect of dissipation on the static characteristics of a non-Bloch system. When $\alpha = 1$ [left panel of Fig. 1(b)], no LBM region exists. Under the action of the NHSE, all bulk modes accumulate at the left boundary of the system. If $\alpha \neq 1$ [middle and right panels of Fig. 1(b)], LBMs divide the system into different regions, and the NHSE acts separately in each region, causing the eigenstates in each region to accumulate on its individual left boundary. Specifically, we find a class of nonlocal skin modes confined to the LBM regions and accumulate them at their corresponding left boundaries, as depicted by the blue lines in Fig. 1(b). These singular modes can be considered NHSE actions on LBMs and are thus called non-Hermitian LBMs. In summary, for a nonlocal system (1) with finite dissipation $\gamma \neq 0$, the NHSE no longer pushes all eigenstates to accumulate at the system boundaries but rather at the boundaries of different LBM regions. This multipartite static configuration can lead to novel quantum walker dynamics.

Note that all sites of the A (B) sublattice and their hoppings form a zero-dimensional directed graph [Fig. 1(a)], where the edge directions are related to the hopping phases for the global hopping case. The left (right) boundary of the system can be defined as a unit composed of the starting (ending) point of the directed graph formed by the A sublattice and the ending (starting) point of the directed graph formed by the B sublattice.

Quantum Walk. We consider a quantum walker with an initial position x_0 in the A sublattice, i.e., $|\psi_{\rm A}(x, t = 0)| = \delta_{x,\,x_0}$ and $|\psi_{\rm B}(x, t = 0)| = 0$, where $\psi_{\rm A}(x) = \langle x, A|\psi\rangle$ and $\psi_{\rm B}(x) = \langle x, B|\psi\rangle$ represent the wave functions of the quantum walker $|\psi\rangle$ distributed in the A and B sublattices, respectively. Due to the presence of a pure loss $(-i\gamma b_j^\dagger b_j)$ in the B sublattice, the quantum walker can escape when accessing a B site. The time evolution of $|\psi(t)\rangle$ satisfies the Schrödinger equation $i\frac{d}{dt}|\psi\rangle = H|\psi\rangle$, which is given by

$$i\frac{d\psi_{\rm A}(x)}{dt} = t_0\psi_{\rm B}(x) + \sum_{l=1}^{R}\frac{t_l}{2}\Big[i\psi_{\rm A}(x-l) - i\psi_{\rm A}(x+l) + \psi_{\rm B}(x-l) + \psi_{\rm B}(x+l)\Big], \tag{3}$$

$$i\frac{d\psi_{\rm B}(x)}{dt} = t_0\psi_{\rm A}(x) + \sum_{l=1}^{R}\frac{t_l}{2}\Big[i\psi_{\rm B}(x+l) - i\psi_{\rm B}(x-l) + \psi_{\rm A}(x-l) + \psi_{\rm A}(x+l)\Big] - i\gamma\psi_{\rm B}(x). \tag{4}$$

The loss of particles can be described by the changing rate of the wave function norm $R(t) = -\frac{d}{dt}\langle\psi|\psi\rangle = -i\langle\psi|H^\dagger - H|\psi\rangle = \sum_x r_x(t)$, where $r_x(t) = 2\gamma|\psi_{\rm B}(x)|^2$ denotes the decay rate at the x-th site in the B sublattice. Over time, the quantum walker completely escapes from the lossy system. Therefore, the escape probability at the x-th cell $P_x = 2\gamma\int_0^\infty dt|\psi_{\rm B}(x)|^2$ satisfies $\sum_x P_x = 1$.

Intuitively, the walker would primarily escape from the sites in the vicinity of its initial location. However, for a system with nearest-neighbor coupling ($R = 1$), there is a high probability that the quantum walker will escape at the boundary far from the initial position under the combined action of NHSE and imaginary gap closing.[23] For a non-Bloch system with infinite-range coupling, i.e., $\alpha \neq 0$, the dynamics of quantum walkers can be more complex. However, due to the lack of analytical solutions for nonlocal systems with infinite-range hopping, in the following section, we primarily rely on numerical simulations to investigate the anomalous quantum dynamics therein.

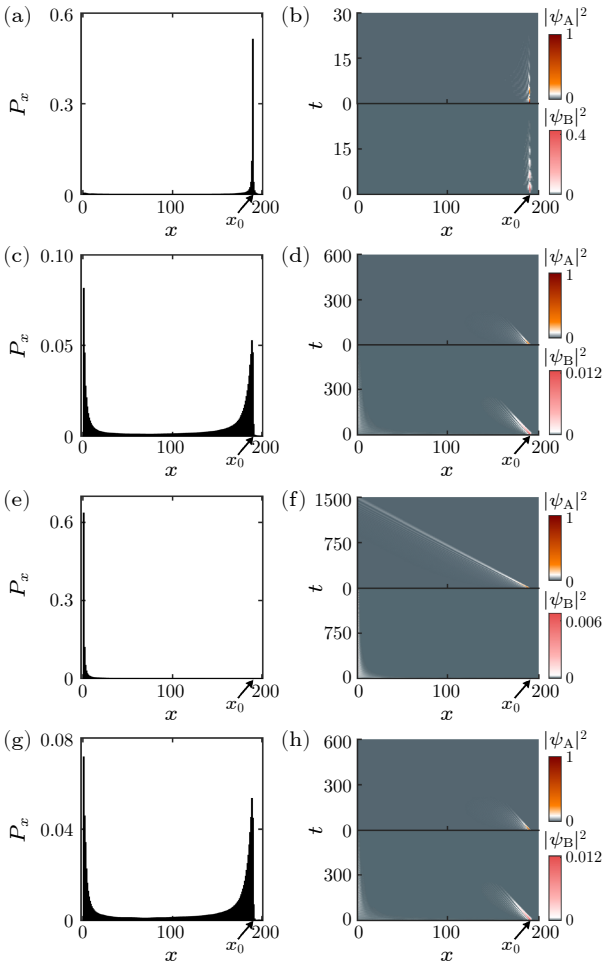

Fig. 2. Escape probability distribution P_x of quantum walker initially located at $x_0 = 190$ (arrows) with (a) $t_0 = 1$, (c) $t_0 = 0.31$, (e) $t_0 = 0.25$, and (g) $t_0 = 0.19$. The evolution of the density distribution in A and B sublattices is depicted in the top and bottom panels of Figs. 3(b), 3(d), 3(f), and 3(h) for the corresponding parameters. Here, the coupling is global with $\alpha = 1$. The other parameters used here are $N = 200$, $\gamma = 0.2$, and $t_l = 0.5$ for $1 \leq l \leq N-1$.

Complete NHEB and Hopping Resonance. First, we focus on the special situation with $\alpha = 1$, i.e., the coupling is global. The system does not support any LBM in its single-particle spectrum, and all eigenstates accumulate at the boundary, as depicted in Fig. 1(b). In the case of $t_0 \gg t_1$, the quantum walker almost escapes near its initial position [Fig. 2(a)]. As t_0 decreases but remains greater than $t_1/2$, the probability for the quantum walker to escape at the boundary starts to increase, as depicted in Fig. 2(c). When t_0 further decreases to the special point $t_1/2$, the quantum walker almost completely escapes from

the boundary [Fig. 2(e)]. For even smaller t_0, the loss probability at the initial point is restored to a finite part, as shown in Fig. 2(g).

To understand the results of P_x, we analyze the density profiles (modulus square) $|\psi_{\rm A}|^2$ and $|\psi_{\rm B}|^2$ of the quantum walker $|\psi\rangle$ on the A and B sublattices, respectively. The results are presented in Figs. 2(b), 2(d), 2(f), and 2(h) for the corresponding cases. Note that although the wave packet of the A sublattice always moves toward the left edge with a nearly uniform speed, the B-sublattice wave function $\psi_{\rm B}$ exhibits different motion patterns with different t_0 values. Considering that the decay rate P_x is determined by $|\psi_{\rm B}|$, these results are consistent with the anomalous loss behavior shown in the left panels of Fig. 2.

We observe that the quantum walker is initially placed in the A sublattice, and the B-sublattice wave function $\psi_{\rm B}$ largely depends on the conversion of the A-sublattice wave function $\psi_{\rm A}$. For each unit cell, the intracell (t_0) and intercell (t_1) hoppings reflect the local and nonlocal conversions between $\psi_{\rm A}$ and $\psi_{\rm B}$, respectively. The competition between local and nonlocal conversions leads to different dynamic behaviors of $\psi_{\rm B}$. When t_0 is large, local conversion dominates, and the distribution of $\psi_{\rm B}$ is identical to that of $\psi_{\rm A}$ [Fig. 2(b)]. Specifically, $\psi_{\rm B}$ is largely distributed near the initial point, and the quantum walker primarily escapes at that position. The influence of nonlocal conversion increases as t_0 decreases. Owing to the presence of all-to-all coupling, $\psi_{\rm B}$ is not only distributed near the initial point but also at positions far away from the initial point and gradually shifts to the left because of the NHSE [Fig. 2(d)]. When $t_0 = t_1/2$, we obtain $i\partial_t\psi_{\rm B}(x) = t_0\sum_y \psi_{\rm A}(y) + t_0\sum_{l=1}[i\psi_{\rm B}(x+l) - i\psi_{\rm B}(x-l)] - i\gamma\psi_{\rm B}(x)$ from Eq. (4). This means that the A-sublattice wave function equally contributes to any position in the B-sublattice. Consequently, $\psi_{\rm B}$ no longer depends on the initial position but is completely determined by the NHSE, exhibiting leftward-skin behavior [Fig. 2(f)]. Hereafter, the special case of $t_0 = t_1/2$ is referred to as the hopping resonance point. Under this special condition, the wave functions of the A and B sublattices differ significantly. As t_0 further decreases, the resonance condition is broken and the complete edge burst disappears, as shown in Figs. 2(g) and 2(h).

Nonlocal Multipartite Escape. Next, we discuss the more general case of $0 < \alpha < 1$. The existence of non-Hermitian LBMs [Fig. 1(b)] can lead to more complex dynamic behaviors. Typical results for a quantum walker initially placed at points in regions without and with LBMs are illustrated in Figs. 3 and 4. In these two plots, we set $\alpha = 0.8$; two LBM regions are located on both ends of the system and separated by distance R (shaded areas), and a non-LBM region is located between them.

Here, we investigate the case in which the quantum walker is initially placed within the middle non-LBM region. Based on the Schrödinger equations (3) and (4), possible phenomena can be predicted. When $x \in [N - R, R + 1]$, the terms $\sum_{l=1}^{R}\psi_{\rm A/B}(x \pm l)$ of the Schrödinger equation have the same form as in the case of $\alpha = 1$. In the thermodynamic limit, this region corresponds to the non-LBM region. Thus, we expect the quantum walker to move similarly to its movement in the case of $\alpha = 1$ when it is initially placed within the non-LBM region. Specifically, at the hopping resonance point with $t_0 = t_1/2$, a complete NHEB effect should be observed, i.e., the escape probability P_x [Fig. 3(e)] and B-sublattice density distribution $|\psi_{\rm B}|^2$ [Fig. 3(f)] accumulate at the left boundary in the non-LBM region and have negligible amplitudes at the initial point x_0. This speculation is confirmed by numerical simulation and demonstrated in Fig. 3, In addition, if t_0 is not too large [Fig. 3(c)–3(f)], the quantum walker exhibits a nonlocal dynamic correlation in the two LBM regions, as confirmed by both the loss probability (left panels) and density distributions (right panels).

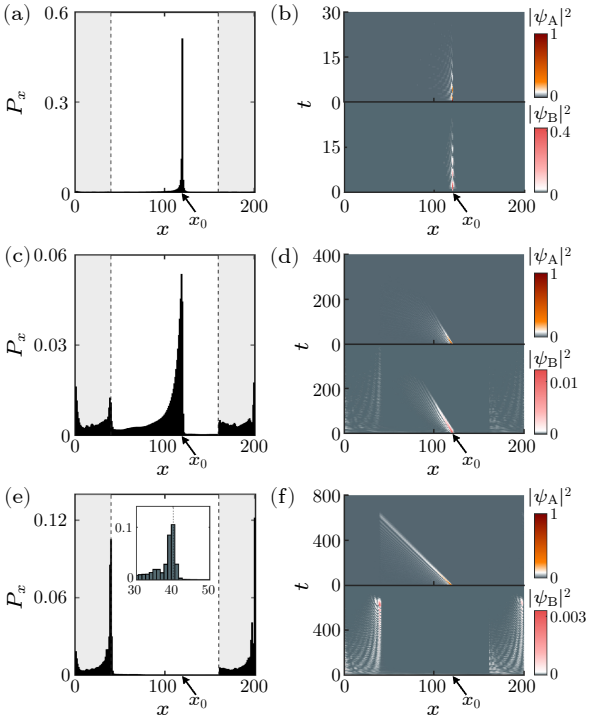

Fig. 3. Escape probability P_x of quantum walker with initial position $x_0 = 120$ (arrows) in non-LBM region (middle white) with (a) $t_0 = 1$, (c) $t_0 = 0.31$, and (e) $t_0 = 0.25$. The shaded areas are the LBM regions. The corresponding A- and B-sublattice density distributions as functions of time t are shown in (b), (d), and (f). The inset of (e) shows the escape probability near the left boundary of the non-LBM region. The other parameters used here are $N = 200$, $\alpha = 0.8$, $\gamma = 0.2$, and $t_l = 0.5$ for $1 \le l \le R$.

To qualitatively understand the phenomenon shown in Fig. 3, particularly the different behaviors of the quantum walker placed in different regions, we can expand the quantum state of the walker based on single-particle eigenstates, i.e., $|\psi(t)\rangle = \sum_n e^{-iE_n t}\langle n_{\rm L}|x_0, A\rangle|n_{\rm R}\rangle$, where $|n_{\rm R}\rangle$ and $|n_{\rm L}\rangle$ denote the right and left eigenvectors of the Hamiltonian, respectively, and E_n denotes the corresponding eigenvalue. According to the middle of Fig. 1(b), the non-LBM eigenstates are mostly located on the left side of the non-LBM region, similar to $\alpha = 1$, and have finite components in the two LBM regions. Thus, the dynamical behavior of the quantum walker in the non-LBM

region is similar to that of $\alpha = 1$, and in the cases of slower dissipation, the quantum walker also escapes in the LBM regions with a probability [Fig. 3(c)–3(f)]. Notably, the escape probability distribution P_x in the non-LBM region accumulates at the left boundary under the resonance condition $t_0 = t_1/2$, exhibiting a complete NHEB in the non-LBM region [the inset of Fig. 3(e)].

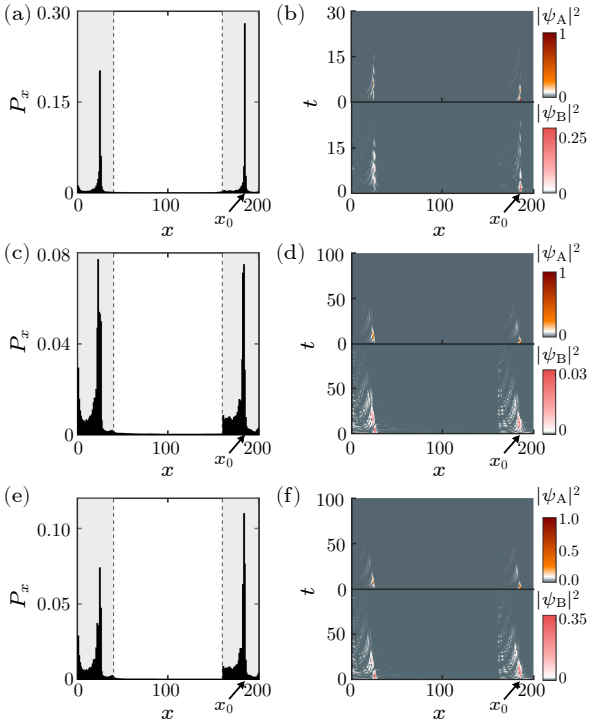

Fig. 4. Escape probability P_x of quantum walker starting at $x_0 = 185$ (arrows) in the right LBM region (shaded) with (a) $t_0 = 1$, (c) $t_0 = 0.31$, and (e) $t_0 = 0.25$. The corresponding A- and B-sublattice density profiles as functions of time t are shown in (b), (d), and (f). The other parameters used here are the same as in Fig. 3.

A quantum walker originally placed in the LBM region is depicted in Fig. 4. In this case, there is no significant difference in the quantum dynamics for different choices of t_0. The most interesting finding is that both the loss rate and density distribution provide a multipeak configuration, with one peak in each LBM region. This suggests that the quantum walker not only escapes near the initial position but also attenuates to the other LBM region to exhibit nonlocal multipoint escape behavior. The peak values of P_x at different points depend on t_0.

Finally, we discuss the case of $\alpha = 0.43$ and present the results in Fig. 5. In the case of $\alpha < 0.5$, a careful inspection of Eqs. (3) and (4) reveals that it is not possible to find a value of x to reproduce the same form of Schrödinger's equations with $\alpha = 1$, i.e., the dynamics for $\alpha = 1$ may not be recovered. From the numerical simulation plotted in Fig. 5, we conclude that although the multipoint escape behavior is still present, a complete edge burst does not occur, which is consistent with our analysis. In contrast, regardless of the initial position of the quantum walker, the spatial distribution of its escape probability always exhibits multiple nonlocal peaks with a distance of R between neighboring peaks.

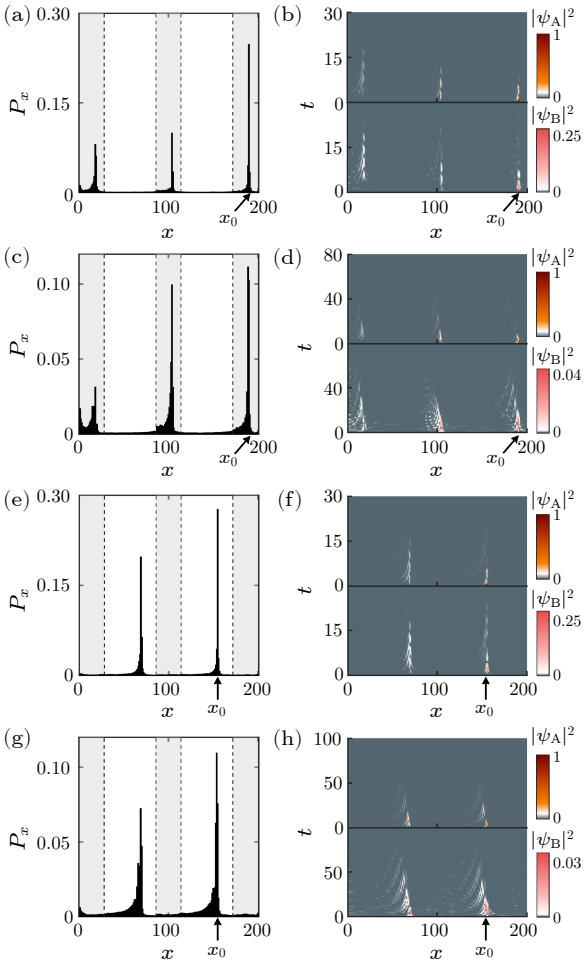

Fig. 5. Escape probability P_x of quantum walker with initial position at (a), (c) $x_0 = 190$ (arrows) in LBM region and (e), (g) $x_0 = 155$ (arrows) in non-LBM region. The corresponding A- and B-sublattice density profiles as functions of time t are plotted in the right column. The hopping parameters $t_0 = 1$ and $t_0 = 0.25$ are represented in the first and third rows and the second and fourth rows, respectively. The other parameters used here are $N = 200$, $\alpha = 0.43$, $\gamma = 0.2$, and $t_l = 0.5$ for $1 \le l \le R$.

Conclusions. In this study, we discuss the static and dynamic properties of a one-dimensional non-Hermitian system with infinite-range hopping, where the hopping range R is comparable to and goes to infinity with the system size N in the thermodynamic limit. Nonlocal coupling can stabilize a novel type of single-particle eigenstate called LBMs, which are distributed only in equally distantly separated spatial domains. Under the NHSE, these modes are pushed to the boundary of their corresponding domains, leading to a multipartite NHSE. For the dynamic properties, we consider a quantum walker initially placed at a single site and analyze the probability distribution of the walker to escape from the system. Owing to the multipartite density distribution induced by nonlocal coupling, the loss probability in general has a multipeak structure, i.e., the walker has a high probability of escaping at multiple spatially separated locations even though it is initially

placed at a single site. More interestingly, we find that if the coupling range is longer than half of the system, i.e., $(R+1)/N \geq 0.5$, the system can present a complete edge burst in the non-LBM region under resonance hopping conditions, where the quantum walker almost completely escapes near the edge in the non-LBM region.

Non-Hermitian LBMs and multipartite escape are novel phenomena unique to this nonlocal system with infinite-range non-global coupling and have not been observed in previous long-range systems with power-law decay coupling. The experimental demonstration of these novel phenomena is interesting, and several experimental platforms to select from include Rydberg atoms[44] and circuit lattices.[45] In particular, circuits can simulate hopping in almost any form or range due to the freedom of circuit connections. In brief, our results demonstrate anomalous dynamical behaviors resulting from the interplay between non-Hermitian and nonlocal couplings and may attract more theoretical and experimental attention to such nonlocal systems.

Acknowledgements. This work was supported by the National Natural Science Foundation of China (Grant Nos. 12074428 and 92265208) and the National Key R&D Program of China (Grant No. 2022YFA1405300).

References

[1] Ashida Y, Gong Z, and Ueda M 2020 *Adv. Phys.* **69** 249
[2] Rotter I 2009 *J. Phys. A: Math. Theor.* **42** 153001
[3] Malzard S, Poli C, and Schomerus H 2015 *Phys. Rev. Lett.* **115** 200402
[4] Leykam D, Bliokh K Y, Huang C, Chong Y D, and Nori F 2017 *Phys. Rev. Lett.* **118** 040401
[5] Song F, Yao S, and Wang Z 2019 *Phys. Rev. Lett.* **123** 170401
[6] Ding L, Shi K, Zhang Q, Shen D, Zhang X, and Zhang W 2021 *Phys. Rev. Lett.* **126** 083604
[7] Ding L, Shi K, Wang Y, Zhang Q, Zhu C, Zhang L, Yi J, Zhang S, Zhang X, and Zhang W 2022 *Phys. Rev. A* **105** L010204
[8] Song F, Yao S, and Wang Z 2019 *Phys. Rev. Lett.* **123** 246801
[9] Yao S and Wang Z 2018 *Phys. Rev. Lett.* **121** 086803
[10] Xiong Y 2018 *J. Phys. Commun.* **2** 035043
[11] Lee C H and Thomale R 2019 *Phys. Rev. B* **99** 201103
[12] Xiao L, Deng T, Wang K, Zhu G, Wang Z, Yi W, and Xue P 2020 *Nat. Phys.* **16** 761
[13] Okuma N, Kawabata K, Shiozaki K, and Sato M 2020 *Phys. Rev. Lett.* **124** 086801
[14] Zhang K, Yang Z, and Fang C 2020 *Phys. Rev. Lett.* **125** 126402
[15] Xin H, Song W, Wu S, Lin Z, Zhu S, and Li T 2023 *Phys. Rev. B* **107** 165401
[16] Longhi S 2022 *Phys. Rev. Lett.* **128** 157601
[17] Hasan M Z and Kane C L 2010 *Rev. Mod. Phys.* **82** 3045
[18] Qi X L and Zhang S C 2011 *Rev. Mod. Phys.* **83** 1057
[19] Kawabata K, Shiozaki K, Ueda M, and Sato M 2019 *Phys. Rev. X* **9** 041015
[20] Rudner M S and Levitov L S 2009 *Phys. Rev. Lett.* **102** 065703
[21] Zeuner J M, Rechtsman M C, Plotnik Y, Lumer Y, Nolte S, Rudner M S, Segev M, and Szameit A 2015 *Phys. Rev. Lett.* **115** 040402
[22] Zhan X, Xiao L, Bian Z, Wang K, Qiu X, Sanders B C, Yi W, and Xue P 2017 *Phys. Rev. Lett.* **119** 130501
[23] Xue W T, Hu Y M, Song F, and Wang Z 2022 *Phys. Rev. Lett.* **128** 120401
[24] Wang L, Liu Q, and Zhang Y 2021 *Chin. Phys. B* **30** 020506
[25] Yuce C and Ramezani H 2023 *Phys. Rev. B* **107** L140302
[26] Zhu J, Mao Y L, Chen H, Yang K X, Li L, Yang B, Li Z D, and Fan J 2024 *Phys. Rev. Lett.* **132** 203801
[27] Xiao L, Xue W T, Song F, Hu Y M, Yi W, Wang Z, and Xue P 2024 *Phys. Rev. Lett.* **133** 070801
[28] Monroe C, Campbell W C, Duan L M, Gong Z X, Gorshkov A V, Hess P W, Islam R, Kim K, Linke N M, Pagano G, Richerme P, Senko C, and Yao N Y 2021 *Rev. Mod. Phys.* **93** 025001
[29] Tan W L, Becker P, Liu F, Pagano G, Collins K S, De A, Feng L, Kaplan H B, Kyprianidis A, Lundgren R, Morong W, Whitsitt S, Gorshkov A V, and Monroe C 2021 *Nat. Phys.* **17** 742
[30] Yan B, Moses S A, Gadway B, Covey J P, Hazzard K R A, Rey A M, Jin D S, and Ye J 2013 *Nature* **501** 521
[31] Moses S A, Covey J P, Miecnikowski M T, Jin D, and Ye J 2017 *Nat. Phys.* **13** 13
[32] Saffman M, Walker T G, and Mølmer K 2010 *Rev. Mod. Phys.* **82** 2313
[33] Mottl R, Brennecke F, Baumann K, Landig R, Donner T, and Esslinger T 2012 *Science* **336** 1570
[34] Norcia M A, Lewis-Swan R J, Cline J R K, Zhu B, Rey A M, and Thompson J K 2018 *Science* **361** 259
[35] Muniz J A, Barberena D, Lewis-Swan R J, Young D J, Cline J R K, Rey A M, and Thompson J K 2020 *Nature* **580** 602
[36] Majer J, Chow J M, Gambetta J M, Koch J, Johnson B R, Schreier J A, Frunzio L, Schuster D I, Houck A A, Wallraff A, Blais A, Devoret M H, Girvin S M, and Schoelkopf R J 2007 *Nature* **449** 443
[37] Wang K, Chen Y, Kadic M, Wang C, and Wegener M 2022 *Commun. Mater.* **3** 35
[38] Sirota L, Ilan R, Shokef Y, and Lahini Y 2020 *Phys. Rev. Lett.* **125** 256802
[39] Defenu N, Donner T, Macrì T, Pagano G, Ruffo S, and Trombettoni A 2023 *Rev. Mod. Phys.* **95** 035002
[40] Hauke P and Tagliacozzo L 2013 *Phys. Rev. Lett.* **111** 207202
[41] Richerme P, Gong Z X, Lee A, Senko C, Smith J, Foss-Feig M, Michalakis S, Gorshkov A V, and Monroe C 2014 *Nature* **511** 198
[42] Shi K, Tian M, Sun F X, and Zhang W 2023 *Phys. Rev. B* **107** 205154
[43] Lee T E 2016 *Phys. Rev. Lett.* **116** 133903
[44] Eckner W J, Darkwah Oppong N, Cao A, Young A W, Milner W R, Robinson J M, Ye J, and Kaufman A M 2023 *Nature* **621** 734
[45] Chen T, Zou D, Zhou Z, Wang R, Feng Y, Sun H, and Zhang X 2024 *Natl. Sci. Rev.* **11** nwae278